

# Cosmological Reionization<sup>1</sup>

Paul R. Shapiro

*Dept. of Astronomy, The University of Texas, Austin, TX 78712 USA*

**Abstract.** The universe was reionized by redshift  $z \approx 6$  by a small fraction of the baryons in the universe, which released energy following their condensation out of a cold, dark, and neutral IGM into the earliest galaxies. The theory of this reionization is a critical missing link in the theory of galaxy formation. Its numerous observable consequences include effects on the spectrum, anisotropy and polarization of the cosmic microwave background and signatures of high-redshift star and quasar formation. This energy release also created feedback on galaxy formation which left its imprint on the mass spectrum and internal characteristics of galaxies and on the gas between galaxies long after reionization was complete. Recent work suggests that the photoevaporation of dwarf galaxy minihalos may have consumed most of the photons required to reionize the currently-favored  $\Lambda$ CDM universe. We will review recent developments in our understanding of this process.

## I INTRODUCTION

Observations of quasar absorption spectra indicate that the universe was reionized prior to redshift  $z = 5$  (e.g. [68]). CMB anisotropy data on the first acoustic peak set limits on the electron scattering optical depth of a reionized IGM which imply  $z_{\text{rei}} \lesssim 40$  (model-dependent) [26]. Together with the lack of a hydrogen Ly $\alpha$  resonance scattering (“Gunn-Peterson”) trough in the spectrum of an SDSS quasar discovered at  $z = 5.8$  [19], these limits currently suggest that  $6 \lesssim z_{\text{rei}} \lesssim 40$ . The origin and consequences of this reionization are among the major unsolved problems of cosmology. (For prior reviews and further references, see, e.g. [3,29,55].) Photons emitted by hitherto undetected massive stars or miniquasars formed within early galaxies are generally thought to be the reionization source.

This is consistent with the theoretical expectation in cosmological models like the Cold Dark Matter (CDM) model, in which the first objects to condense out of the background and possibly begin star formation were small, of subgalactic mass (i.e.  $M \lesssim 10^6 M_\odot$ ) and began to form as early as  $z \gtrsim 30$  (e.g. [25,30,57,71]). The initial collapse of such objects only led to star formation if radiative cooling

---

<sup>1)</sup> Invited Paper, Plenary Session, to appear in *Proceedings of the 20<sup>th</sup> Texas Symposium on Relativistic Astrophysics and Cosmology*, eds. H. Martel and J. C. Wheeler (AIP Conference Series), in press (2001).

was possible after collapse, usually involving  $\text{H}_2$  molecules, and it is likely that the first objects to form stars released radiation (and possibly SN explosion energy as well) which exerted a strong feedback on the subsequent formation history of other objects. The details of this feedback and even the overall *sign* (i.e. negative or positive) are poorly understood (e.g. [8,14,17,20,28,31,32,36,55,57,59]). It appears that the first stars would have photodissociated  $\text{H}_2$  long before enough UV was emitted to bring about reionization, so it is currently thought that if reionization was accomplished by stars, they formed in objects with virial temperature  $T_{\text{vir}} > 10^4\text{K}$ , of mass  $\gtrsim 10^8 M_\odot$ , which were able to cool by atomic radiative cooling, even without  $\text{H}_2$ . This conclusion changes, however, if the first sources were miniquasars whose nonthermal spectra had a significant X-ray flux, since this would have created a *positive* feedback on the  $\text{H}_2$ .

If we adopt an optimum efficiency for massive star formation and radiation release by the collapsed baryon fraction in a standard CDM model which is flat, matter-dominated, and COBE-normalized (an unrealistic model which has too high an amplitude to satisfy X-ray cluster abundance constraints at  $z = 0$ , but conservatively overestimates  $z_{\text{rei}}$ ),  $z_{\text{rei}} \approx 50$  is possible [55]. But more suitable CDM models all tend to yield  $z_{\text{rei}} \lesssim 20$  (e.g. [4,13,15,25,30,57,74]).

## II COSMOLOGICAL IONIZATION FRONTS

**Ionization Fronts in a Clumpy Universe.** The neutral, opaque IGM out of which the first bound objects condensed was dramatically reheated and reionized at some time between a redshift  $z \approx 50$  and  $z \approx 6$  by the radiation released by some of these objects. When the first sources turned on, they ionized their surroundings by propagating weak, R-type ionization fronts which moved outward supersonically with respect to both the neutral gas ahead of and the ionized gas behind the front, racing ahead of the hydrodynamical response of the IGM [54,56]. The problem of the time-varying radius of a spherical I-front which surrounds isolated sources in a cosmologically-expanding IGM was solved analytically by [54,56], taking proper account of the I-front jump condition generalized to cosmological conditions. They applied these solutions to determine when and how fast these I-front-bounded spheres would grow to overlap and, thereby, complete the reionization of the universe. The effect of density inhomogeneity on the rate of I-front propagation was described by a mean “clumping factor”  $c_l > 1$ , which slowed the I-fronts by increasing the average recombination rate per H atom inside clumps. This suffices to describe the average rate of I-front propagation as long as the clumps are either not self-shielding or, if so, only absorb a fraction of the ionizing photons emitted by the central source. In two recent calculations, this analytical prescription was adapted to N-body simulations of structure formation in the CDM model, to calculate the evolving size of the spherical H II regions with which to surround putative sources of ionizing radiation, to model the growth of the ionized volume filling factor leading to reionization [4,15].

Numerical radiative transfer methods are currently under development to solve this problem in 3D for the inhomogeneous density distribution which arises as cosmic structure forms, but so far are limited to an imposed density field without gas dynamics (e.g. [1,16,45,51]). A different approach, which replaces radiative transfer with a “local optical depth approximation,” intended to mimic the average rate at which I-fronts expanded and overlapped during reionization within the context of cosmological gas dynamics simulation, has also been developed [22]. These recent attempts to model inhomogeneous reionization numerically are handicapped by their limited spatial resolution ( $\gtrsim 1$  kpc), which prevents them from resolving the most important density inhomogeneities. The dynamical response of density inhomogeneities to the I-fronts which encountered them and the effect which these inhomogeneities had, in turn, on the progress of universal reionization, therefore, require further analysis. Toward this end, we have developed a radiation-hydrodynamics code which incorporates radiative transfer and have focused our attention on properly resolving this small-scale structure. In what follows, we summarize the results of new radiation-hydrodynamical simulations of what happens when a cosmological I-front overtakes a gravitationally-bound density inhomogeneity – a dwarf galaxy minihalo – during reionization. According to [27], the photoevaporation of these sub-kpc-sized objects is likely to be the dominant process by which ionizing photons were absorbed during reionization, so this problem is of critical importance in determining how reionization proceeded.

**Dwarf Galaxy Minihalos at High Redshift.** The effect which small-scale clumpiness had on reionization depended upon the sizes, densities, and spatial distribution of the clumps overtaken by the I-fronts during reionization. For the currently-favored  $\Lambda$ CDM model ( $\Omega_0 = 1 - \lambda_0 = 0.3$ ,  $h = 0.7$ ,  $\Omega_b h^2 = 0.02$ , primordial power spectrum index  $n_p = 1$ ; COBE-normalized), the universe at  $z > 6$  was already filled with dwarf galaxies capable of trapping a piece of the global, intergalactic I-fronts which reionized the universe and photoevaporating their gaseous baryons back into the IGM (see Figure 1). Prior to their encounter with these I-fronts, “minihalos” with  $T_{\text{vir}} < 10^4$  K were neutral and optically thick to hydrogen ionizing radiation, as long as their total mass exceeded the Jeans mass  $M_J$  in the unperturbed background IGM prior to reionization [i.e.  $M_J = 5.7 \times 10^3 (\Omega_0 h^2 / 0.15)^{-1/2} (\Omega_b h^2 / 0.02)^{-3/5} ((1+z)/10)^{3/2} M_\odot$ ], as was required to enable baryons to collapse into the halo along with dark matter. Their “Strömgren numbers”  $L_S \equiv 2R_{\text{halo}}/\ell_S$ , the ratio of a halo’s diameter to its Strömgren length  $\ell_S$  inside the halo (the length of a column of gas within which the unshielded arrival rate of ionizing photons just balances the total recombination rate), were large. For a uniform gas of H density  $n_{H,c}$ , located a distance  $r_{\text{Mpc}}$  (in Mpc) from a UV source emitting  $N_{\text{ph},56}$  ionizing photons (in units of  $10^{56} \text{s}^{-1}$ ), the Strömgren length is only  $\ell_S \approx (100 \text{ pc}) (N_{\text{ph},56} / r_{\text{Mpc}}^2) (n_{H,c} / 0.1 \text{ cm}^{-3})^{-2}$ , so  $L_S \gg 1$  for a wide range of halo masses and sources of interest. In that case, the intergalactic, weak, R-type I-front which entered each minihalo during reionization would have decelerated to about twice the sound speed of the ionized gas before it could exit the other side, thereby transforming itself into a D-type front, preceded by a shock. Typically, the

side facing the source would then have expelled a supersonic wind backwards toward the source, which shocked the surrounding IGM as the minihalo photoevaporated.

The importance of this photoevaporation process has long been recognized in the study of interstellar clouds exposed to ionizing starlight (e.g. [5,6,38,39,41,43,47,53,69]). In the cosmological context, however, its importance has only recently been fully appreciated.

In proposing the expanding minihalo model to explain Ly $\alpha$  forest (“LF”) quasar absorption lines, [9] discussed how gas originally confined by the gravity of dark-matter minihalos in the CDM model would have been expelled by pressure forces if photoionization by ionizing background radiation suddenly heated all the gas to an isothermal condition at  $T \approx 10^4 K$ , a correct description only in the optically thin limit. The first discussion of the photoevaporation of a primordial density inhomogeneity overtaken by a cosmological I-front, including radiation-hydrodynamical simulations, however, was in [65,66]. [2] subsequently estimated the relative importance of this process for dwarf galaxy minihalos of different masses at different epochs in the CDM model, concluding that 50%–90% of the gas which had already collapsed into gravitationally bound objects when reionization occurred should have been photoevaporated.

Not only did this photoevaporation during reionization affect most of the collapsed baryons, but so common were minihalos with  $T_{\text{vir}} < 10^4 K$  during reionization that the typical reionizing photon is likely to have encountered one of them, according to [27]. A catalogue of all halos in a cubic volume 100 kpc (50 kpc) on a side at  $z = 9$  in the currently-favored  $\Lambda$ CDM model based on N-body simulations reveals that minihalos with  $T_{\text{vir}} < 10^4 K$  (i.e.  $M < 10^{7.6} M_\odot$ ) were separated on

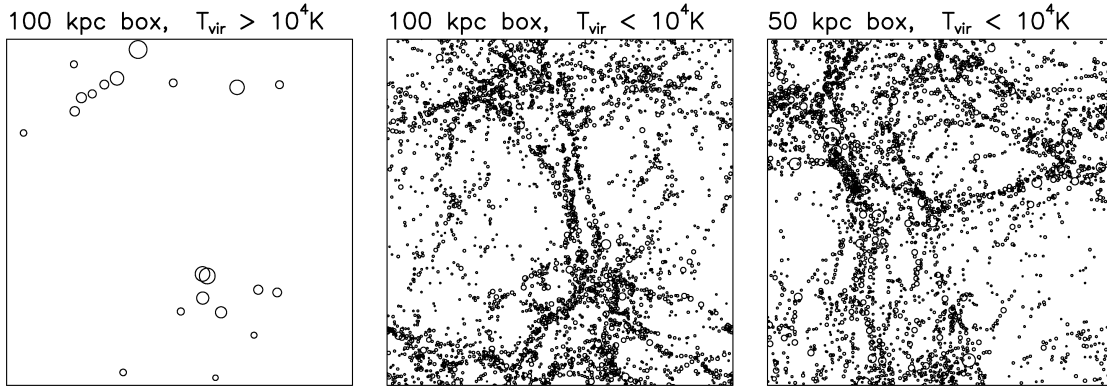


**FIGURE 1.  $\Lambda$ CDM Halos at High Redshift:** DM Halos at  $z = 9$  are shown with sizes and locations determined by FOF algorithm applied to P<sup>3</sup>M simulations ( $128^3$  particles,  $256^3$  cells), projected onto face of simulation cube of proper size  $L_{\text{box}}$ , as labelled. (a) (left)  $M_{\text{halo}} > 10^{7.6} M_\odot$  only (i.e.  $T_{\text{vir}} > 10^4 K$ ). (b) (middle)  $10^{5.6} M_\odot < M_{\text{halo}} < 10^{7.6} M_\odot$  only (i.e.  $T_{\text{vir}} < 10^4 K$ ) – THE MINIHALOS; (c) (right) like (b), but higher resolution simulation with same number of particles and cells in 1/8 volume (i.e.  $M_{\text{halo,min}} = 10^{4.7} M_\odot$ ).

average by only  $d \approx 7$  kpc (3.5 kpc) for  $M \geq 10^{5.6} M_\odot$  ( $M \geq 10^{4.7} M_\odot$ ), respectively, while their geometric cross sections together covered  $f \sim 16\%$  (30%) of the area along every 100 kpc of an average line of sight [60] [see Figs. 1(b), (c)]. If the sources of reionization, on the other hand, were larger-mass halos with  $T_{\text{vir}} > 10^4 K$  [like those in Fig. 1(a)], then these were well-enough separated that typical reionization photons were likely to have been absorbed by intervening photoevaporating minihalos. To demonstrate this in a statistically meaningful way with more dynamic range than the N-body results can yet provide, an analytical approximation to the detailed numerical results is required. We shall combine the well-known Press-Schechter (PS) prescription for deriving the average number density of halos of different mass at each epoch with the nonsingular truncated isothermal sphere (TIS) model of [34,58] for the size, density profile, and temperature of each halo as unique functions of the halo mass and collapse redshift for a given background universe. (The TIS model and further tests and applications of it are briefly mentioned elsewhere in this volume [35]). We illustrate the validity of these approximations in Figure 2 by comparing them with the N-body simulation results depicted in Figure 1. The PS halo mass functions plotted in Figure 2(a) are shown in Figure 2(b) to reproduce the N-body results over a range of  $10^5$  in halo mass, for which  $dn_{\text{halo}}/dM \approx 10^{12} (M/M_\odot)^{-2} \text{Mpc}^{-3} M_\odot$  (proper units) at  $z = 9$ . Likewise, Figure 2(c) shows that the TIS model correctly predicts the average virial ratio,  $[GM_{200}/(\sigma_V^2 r_{200})]_{\text{TIS}} = 2.176$ , for halos of different mass according to the N-body results, over this same mass range.

This TIS+PS approximation allows us to determine which halo masses are sub-

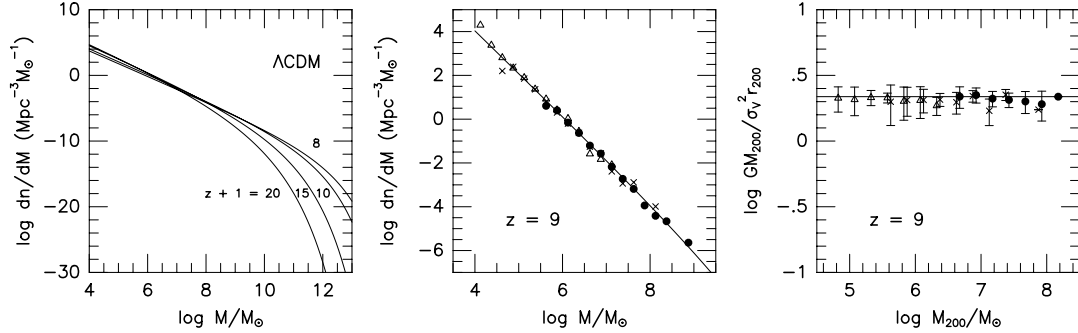


**FIGURE 2. CDM Halos: N-body Results Vs. PS+TIS Approximations:** (a) (left) Proper Number Density of Halos per Unit Halo Mass,  $dn_{\text{halo}}/dM$ , in  $\Lambda$ CDM at different redshifts, as labelled, according to PS approximation; (b) (middle) Same as (a), with PS mass function at  $z = 9$  (solid curve) compared with N-body results for halos in Fig. 1 for three different resolutions:  $L_{\text{box}} = 100$  kpc (circles), 50 kpc (crosses), and 25 kpc (triangles); (c) Virial ratio,  $GM_{200}/(\sigma_V^2 r_{200})$ , versus halo mass  $M_{200}$ , where  $\sigma_V^2$  is the halo DM velocity dispersion and  $M_{200}$  and  $r_{200}$  are the mass and radius of the sphere whose average density is 200 times the cosmic mean value, for all halos in Fig. 1 with at least 200 particles per halo [symbols same as in (b), with  $1\sigma$  error bars]. Horizontal line is analytical prediction of the TIS model.

ject to photoevaporation and how common they are, as functions of redshift. Each minihalo with  $T_{\text{vir}} < 10^4 \text{K}$  is opaque to H-ionizing photons with a geometric cross section  $\sigma_{\text{halo}} = \pi r_t^2$ , where  $r_t$  = TIS radius  $\approx (0.75 \text{ kpc})(M/10^7 M_\odot)^{1/3}[(1 + z_{\text{coll}})/10]^{-1}(\Omega_0 h^2/0.15)^{-1/3}$ . Ionizing photons travelling through this universe will suffer absorption by these minihalos [i.e. those with mass  $M_J \leq M \leq M(10^4 \text{K})$  at each  $z$ ] with a mean free path  $\lambda_{\text{mfp}}$ , as shown in Figure 3(a). For comparison, the mean separation  $\langle d_{\text{sep}} \rangle$  of halos of each mass is plotted in Figure 3(b). At  $z = 9$ , for example,  $\lambda_{\text{mfp}} = 160 \text{ kpc}$ , while halos of mass  $M \gtrsim 10^8 M_\odot$  are separated on average by  $\langle d_{\text{sep}} \rangle \approx 50(M/10^8 M_\odot)^{1/3} \text{ kpc}$ . As shown in Figure 3(c), their ratio,  $\langle d_{\text{sep}} \rangle / \lambda_{\text{mfp}}$ , gives the fraction of the sky, as seen by a source halo of a given mass, which is covered by opaque minihalos located within the mean volume per source halo. If halos with  $M \gtrsim 10^8 M_\odot$  are the reionization sources, their minihalo covering fraction is close to unity and increases with increasing source mass. This estimate will increase by a factor of a few if we take account of the statistical bias by which minihalos tend to cluster around the source halos [27].

An argument like this led [27] to argue that our photoevaporating minihalos are the chief consumers of the ionizing photons responsible for reionization. As a result, they suggest, the photoevaporation of these minihalos drives the number of ionizing photons per baryon required to reionize the universe up by an order of magnitude compared to previous estimates! A recent semi-analytical study of inhomogeneous reionization by [44], which neglected this effect, concluded that only one ionizing photon per hydrogen atom would have been sufficient to reionize most of the volume of the IGM by  $z \approx 5$ , an order of magnitude too low when compared to the new photoevaporation-dominated estimates. The gas clumping model they adopted apparently missed the smallest scales because it was adjusted to match numerical simulation results which could not resolve these scales. Simulations by [22], which agreed with [44], have the same problem since their resolution limit

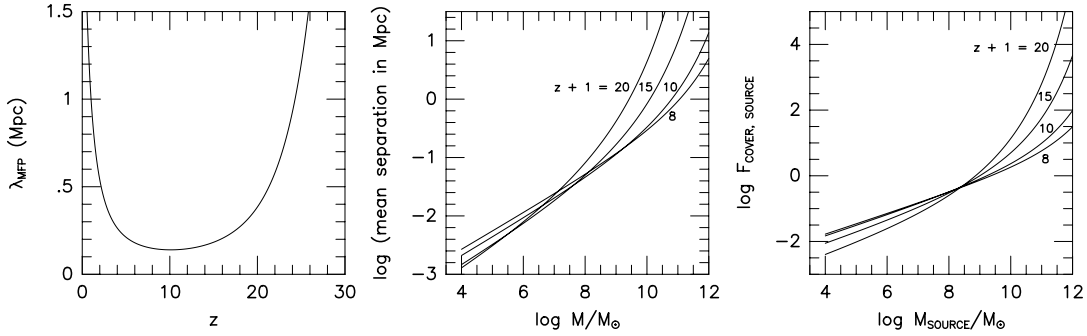


**FIGURE 3. Minihalo Sinks and Sources:** (a) (left) Proper mean free path  $\langle n_{\text{halo}} \sigma_{\text{halo}} \rangle^{-1}$  for absorption of photons by minihalos in  $\Lambda \text{CDM}$  at different  $z$  (i.e. if they photoevaporate at  $z_{\text{ev}} < z$ ); (b) (middle) Proper mean separation of halos  $\langle d_{\text{sep}} \rangle \equiv (M dn_{\text{halo}}/dM)^{-1/3}$  versus halo mass at different redshifts in  $\Lambda \text{CDM}$ , as labelled; (c) (right) Fraction of sky covered by minihalos located within the mean volume per source halo,  $F_{\text{cover,source}} = \langle d_{\text{sep}} \rangle / \lambda_{\text{mfp}}$ , versus source halo mass, at different redshifts.

exceeded  $\sim 1$  kpc, too large to resolve the minihalos which photoevaporate.

*We are led to conclude that further study of the photoevaporation of cosmological minihalos during reionization is essential if we are to advance the theory of reionization.* The new “photoevaporation-dominated” reionization scenario suggests that significantly more than one photon per baryon may have been required, and this is difficult to understand on the basis of simple extrapolation (e.g. [21,42]) of either quasar or stellar photon production rates observed at  $z < 5$  to  $z > 5$ . Perhaps this problem will be alleviated by appeal to the recently revised stellar output for zero metallicity stars [10,73], or to a higher escape fraction of ionizing photons from their source than the nominal  $f_{\text{esc}} \approx 0.1$  typically assumed (e.g. [18,40,52,70,76]). Alternatively, if minihalo sources, alone, reionized the IGM (e.g. with miniquasars instead of starlight), then their ionizing photons could have done so without encountering any other minihalos, since  $F_{\text{cover,source}} < 1$  for halos with  $T_{\text{vir}} < 10^4\text{K}$ . Photons released, thereafter, would have encountered fewer opaque minihalos, as well, since baryons would not then have condensed out of a reheated IGM to form *new* minihalos, according to [57].

The good news is that observations should be able to distinguish these possibilities. In order for photoevaporating minihalos to have consumed most of the ionizing photons produced before reionization is complete, the covering fraction of the ionization sources by these photoevaporative flows must be of order unity. Hence, if we can observe the sources of universal reionization directly, we will generally be able to observe foreground photoevaporating minihalos in absorption toward these sources. Such observations will constrain and help diagnose the reionization process. As shown in Figure 4, photons emitted by *any* high  $z$  source before or during reionization will typically encounter large numbers of photoevaporating minihalos at  $z > 6$ . The number of minihalos probed per unit redshift interval, in fact, is just  $(1+z)^{-1}$  times the ratio of the horizon size  $c/H(t)$  at  $z$  to  $\lambda_{\text{mfp}}$ , a large number. It is important, therefore, for us to predict the effect which reionization will have

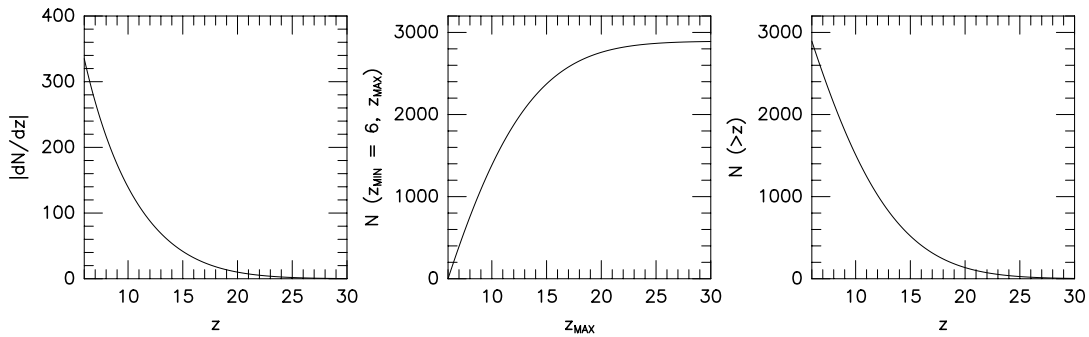


**FIGURE 4. Minihalos Encountered By a Photon Emitted At High Redshift:** (a) (left) Number of minihalos per unit redshift interval in  $\Lambda$ CDM encountered by a photon at redshift  $z$  which travels along the average LOS; (b) (middle) Total number of minihalos in  $\Lambda$ CDM along photon path which probes redshift interval  $z_{\text{min}} \leq z \leq z_{\text{max}}$  for  $z_{\text{min}} = 6$  is plotted versus  $z_{\text{max}}$ ; (c) (right) Asymptotic number of halos along photon path which probes redshift interval  $(z, \infty)$ .

on the gas in these minihalos.

**The Photoevaporation of Dwarf Galaxy Minihalos Overtaken by Cosmological Ionization Fronts.** We have performed radiation-hydrodynamical simulations of the photoevaporation of a cosmological minihalo overrun by a weak, R-type I-front in the surrounding IGM, created by an external source of ionizing radiation [61–64]. The gas contained H, He, and a possible heavy element abundance of  $10^{-3}$  times solar. Our simulations in 2D, axisymmetry used an Eulerian hydro code with Adaptive Mesh Refinement and the Van Leer flux-splitting algorithm, which solved nonequilibrium ionization rate equations (for H, He, C, N, O, Ne, and S) and included an explicit treatment of radiative transfer by taking into account the bound-free opacity of H and He [43,49,50]. The reader is referred to [65–67] for earlier results which considered uniform clouds and demonstrated the importance of a proper treatment of optical depth.

Here we compare some of our results of minihalo photoevaporation in a  $\Lambda$ CDM universe [64] for two types of source spectra: a quasar-like source with emission spectrum  $F_\nu \propto \nu^{-1.8}$  ( $\nu > \nu_H$ ) and a stellar source with a 50,000 K blackbody spectrum, with luminosity and distance adjusted to keep the ionizing photon fluxes the same in the two cases. In particular, if  $r_{\text{Mpc}}$  is the proper distance (in Mpc) between source and minihalo and  $N_{\text{ph},56}$  is the H-ionizing photon luminosity (in units of  $10^{56} \text{ s}^{-1}$ ), then the flux at the location of the minihalo would, if unattenuated, correspond initially to  $N_{\text{ph},56}/r_{\text{Mpc}}^2 = 1$ ; thereafter,  $r_{\text{Mpc}} \propto a(t)$ , the cosmic scale factor.

Our initial condition before ionization is that of a  $10^7 M_\odot$  minihalo in the  $\Lambda$ CDM

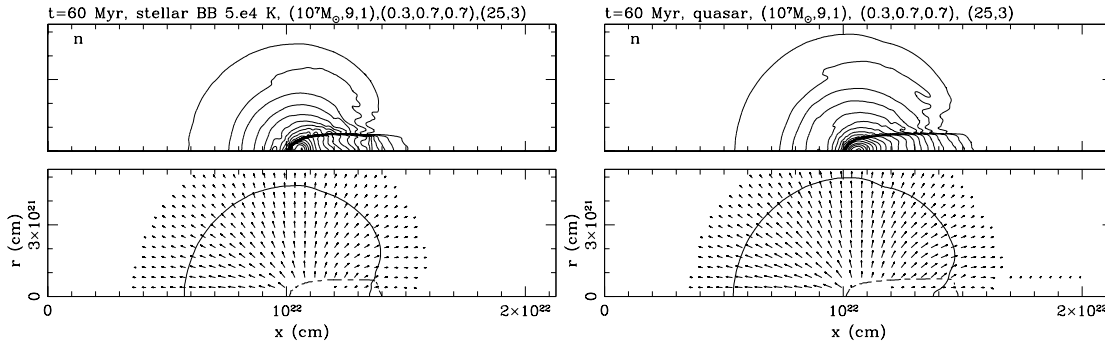


**FIGURE 5. Photoevaporating Minihalo I.** One time-slice, 60 Myr after I-front caused by ionizing source (located far to the left of computational box along the  $x$ -axis) overtakes a  $10^7 M_\odot$  minihalo [centered at  $(r, x) = (0, 1.06 \times 10^{22} \text{ cm})$ ] at  $z = 9$  in the  $\Lambda$ CDM universe, for two types of source spectra: (a) (left) STELLAR CASE and (b) (right) QUASAR CASE. (upper panels) isocontours of atomic density, logarithmically spaced, in  $(r, x)$ -plane of cylindrical coordinates; (lower panels) velocity arrows are plotted with length proportional to gas velocity. An arrow of length equal to the spacing between arrows has velocity  $25 \text{ km s}^{-1}$ ; minimum velocities plotted are  $3 \text{ km s}^{-1}$ . Solid line shows current extent of gas initially inside minihalo at  $z = 9$ . Dashed line is I-front (50% H-ionization contour).



universe which collapsed out and virialized at  $z_{\text{coll}} = 9$ , yielding a truncated, nonsingular isothermal sphere (“TIS”) of radius  $r_t = 0.75$  kpc in hydrostatic equilibrium with  $T_{\text{vir}} = 4000$  K and dark-matter velocity dispersion  $\sigma_V = 5.2 \text{ km s}^{-1}$ . The TIS profile has a central density and an average density which are 18,000 and 130 times the mean background density, respectively, with core radius  $r_0 \equiv r_{\text{King}}/3 \sim r_t/30$ . This hydrostatic sphere is embedded in a self-similar, spherical, cosmological infall according to [7].

The results of our simulations on an  $(r, x)$ -grid with  $256 \times 512$  cells are illustrated by Figures 5–9. The minihalo shields itself against ionizing photons, traps the R-type I-front which enters the halo, causing it to decelerate inside the halo to close to the sound speed of the ionized gas and transform itself into a D-type front, preceded by a shock. The side facing the source expels a supersonic wind backwards towards the source, which shocks the IGM outside the minihalo. The

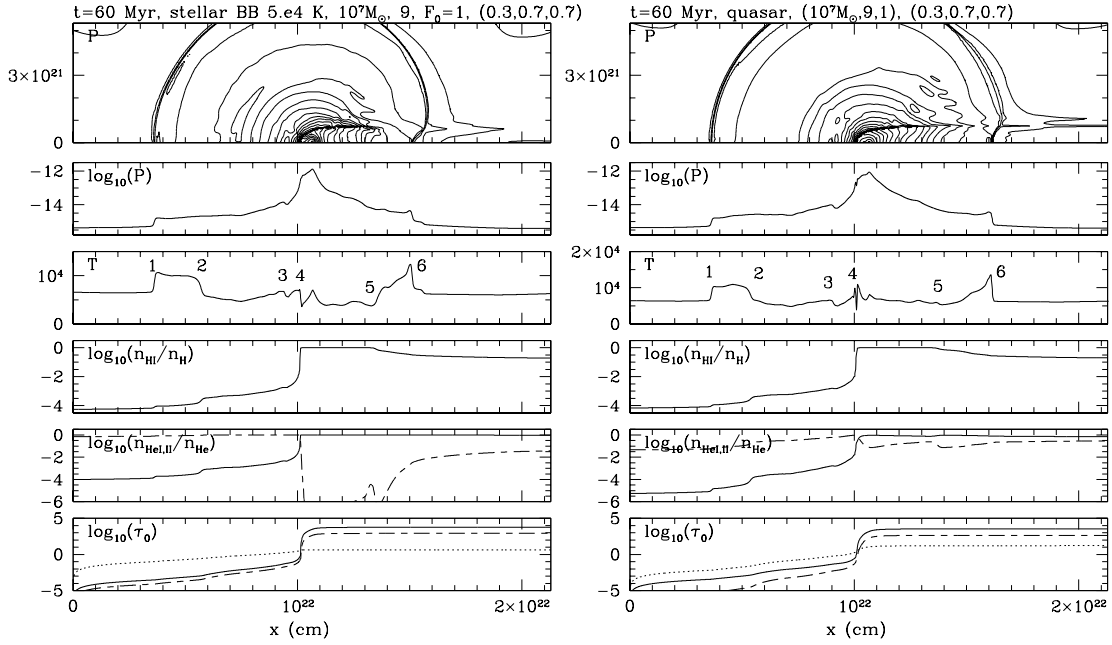


**FIGURE 6. Photoevaporating Minihalo II.** Same time-slice as Fig. 5. (a) (left) STELLAR CASE and (b) (right) QUASAR CASE. From top to bottom: (i) isocontours of pressure, logarithmically spaced, in  $(r, x)$ -plane of cylindrical coordinates; (ii) pressure along the  $r = 0$  symmetry axis; (iii) temperature; (iv) H I fraction; (v) He I (solid) and He II (dashed) fractions; (vi) bound-free optical depth measured from  $x = 0$  along the  $x$ -axis, at the threshold ionization energies for H I (solid), He I (dashed), He II (dotted). Key features of the flow are indicated by the numbers which label them on the temperature plots: 1 = IGM shock; 2 = contact discontinuity which separates shocked halo wind (between 2 and 3) from swept-up IGM (between 1 and 2); 3 = wind shock; between 3 and 4 = supersonic wind; 4 = I-front; 5 = boundary of gas initially inside minihalo at  $z = 9$ ; 6 = shock in shadow region caused by compression of shadow gas by shock-heated gas outside shadow.

wind grows more isotropic with time as the remaining neutral halo material is photoevaporated. Since this gas was initially bound to a dark halo with  $\sigma_V < 10 \text{ km s}^{-1}$ , photoevaporation proceeds unimpeded by gravity. Figures 5 and 6 show the structure of the photoevaporative flow 60 Myrs after the global I-front first overtakes the minihalo, with key features of the flow indicated by the labels on the temperature plot in Figure 6. Figure 7(a) shows how the neutral mass of the gas initially within the original hydrostatic sphere gradually declines as the minihalo photoevaporates, within  $t_{\text{ev}} \approx 250$  (100) Myrs for the stellar (quasar) cases, respectively. The gradual decay of the opaque cross section of the minihalo as seen by the source is illustrated by Figure 7(b).

Some observational signatures of this process are shown in Figures 8 and 9. Figure 8 shows the spatial variation of the relative abundances of C, N, and O ions along the symmetry axis after 60 Myrs. While the quasar case shows the presence at 60 Myrs of low as well as high ionization stages for the metals, the softer spectrum of the stellar case yields less highly ionized gas on the ionized side of the I-front (e.g. mostly C III, N III, O III) and the neutral side as well (e.g. C II, N I, O I and II). The column densities of H I, He I and II, and C IV for minihalo gas of different velocities as seen along the symmetry axis at different times are shown in Figure 9. At early times, the minihalo gas resembles a weak Damped Ly $\alpha$

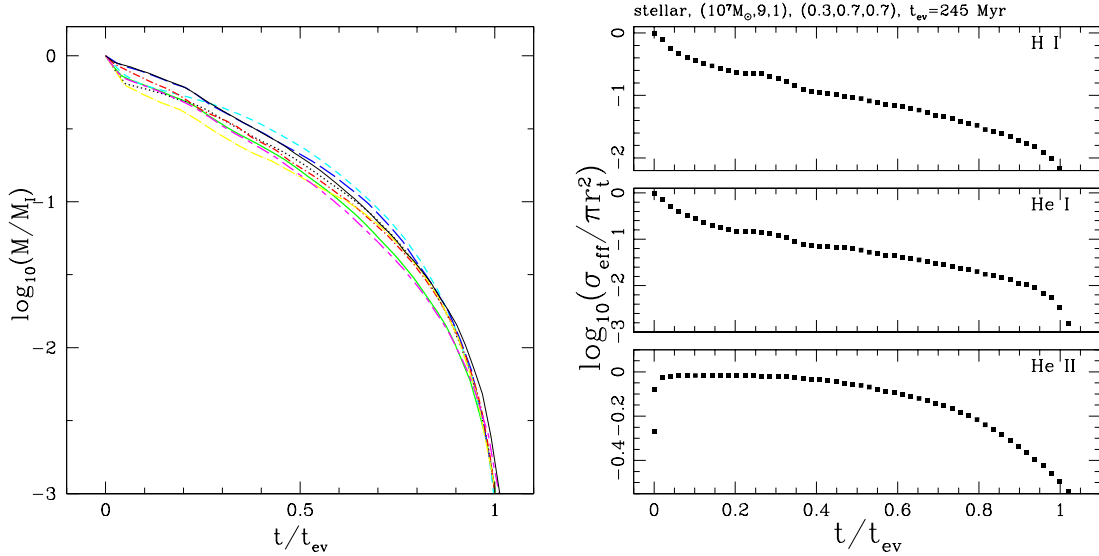


**FIGURE 7. Evolution of Neutral Gas Content of Photoevaporating Minihalo.**

(a) (left) Fraction of mass  $M_I$ , the mass which is initially inside the minihalo when the intergalactic I-front overtakes it, which remains neutral versus time  $t$  (in units of the evaporation time  $t_{\text{ev}}$  at which this  $M/M_I = 10^{-3}$ ), for a large range of cases with different assumed source spectra and fluxes and minihalo masses; (b) (right) fraction of minihalo initial geometric cross section  $\pi r_t^2$  which is opaque to source photons that can ionize H I (top panel), He I (middle panel), or He II (bottom panel) versus time (in units of  $t_{\text{ev}}$ ), for the case with stellar source shown in Figs. 5, 6 ( $t_{\text{ev}} = 245$  Myr).

(“DLA”) absorber with small velocity width ( $\gtrsim 10 \text{ km s}^{-1}$ ) and  $N_{\text{HI}} \gtrsim 10^{20} \text{ cm}^{-2}$ , with a Ly $\alpha$ -Forest(“LF”)-like red wing (velocity width  $\gtrsim 10 \text{ km s}^{-1}$ ) with  $N_{\text{HI}} \gtrsim 10^{16} \text{ cm}^{-2}$  on the side moving toward the source, with a He I profile which mimics that of H I but with  $N_{\text{HeI}}/N_{\text{HI}} \sim [\text{He}]/[\text{H}]$ , and with a weak C IV feature with  $N_{\text{CIV}} \sim 10^{11} (10^{12}) \xi \text{ cm}^{-2}$  for the stellar (quasar) cases, respectively, displaced in

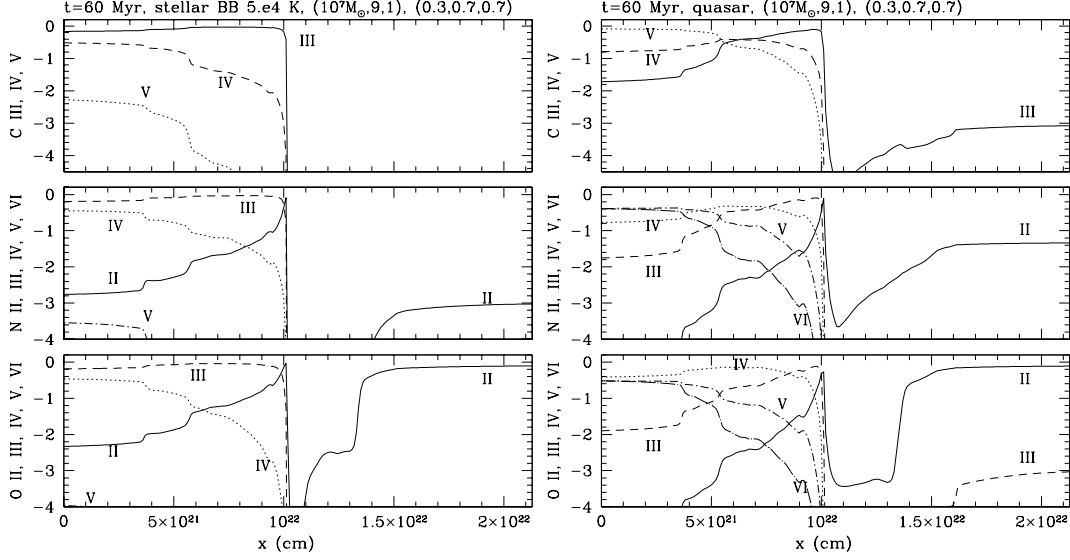


**FIGURE 8. Observational diagnostics I: ionization structure of metals.** C, N, and O ionic fractions along symmetry axis at  $t = 60 \text{ Myr}$ , for photoevaporating minihalo of Figs. 5, 6. (a) (left) STELLAR CASE; (b) (right) QUASAR CASE.

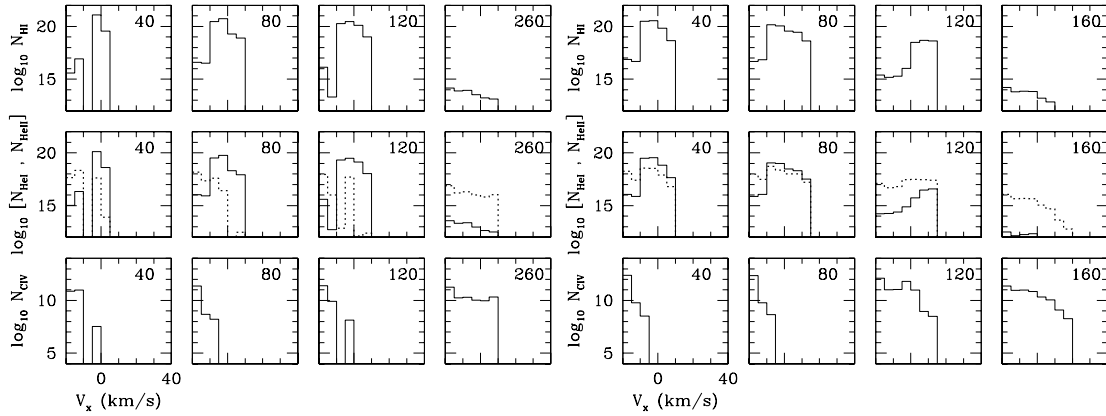


**FIGURE 9. Observational diagnostics II. Absorption lines.** Minihalo column densities ( $\text{cm}^{-2}$ ) along symmetry axis for gas at different velocities, for photoevaporating minihalo of Figs. 5, 6. (a) (left) STELLAR CASE; (b) (right) QUASAR CASE. (Top) H I; (Middle) He I (solid) and He II (dotted); (Bottom) C IV (i.e. if  $[\text{C}]/[\text{C}]_{\odot} = \xi \times 10^{-3}$ , then plotted values are  $N_{\text{CIV}}/\xi$ ). Each box labelled with time (in Myrs) since arrival of intergalactic I-front.

this same asymmetric way from the velocity of peak H I column density, where  $\xi \equiv [C]/[C]_{\odot} \times 10^3$ . For He II at early times, the stellar case has  $N_{\text{HeII}} \approx 10^{18} \text{cm}^{-2}$  shifted by 10's of km/sec to the red of the H I peak, while for the quasar case, He II simply follows the H I profile, except that  $N_{\text{HeII}}/N_{\text{HI}} \approx 10$  in the red wing but  $N_{\text{HeII}}/N_{\text{HI}} \approx 10^{-2}$  in the central H I feature. After 260 (160) Myr, however, only a LF-like H I feature with column density  $N_{\text{HI}} \sim 10^{14} \text{cm}^{-2}$  remains, with  $N_{\text{HeI}}/N_{\text{HI}} \sim 1/4$  ( $\lesssim 1/30$ ),  $N_{\text{HeII}}/N_{\text{HI}} \sim 10^3$  ( $10^2$ ), and  $N_{\text{CIV}}/N_{\text{HI}} \sim 3(1) \times [C]/[C]_{\odot}$  for the stellar (quasar) cases, respectively.

As described above, intervening minihalos like these are expected to be ubiquitous along the line of sight to high redshift sources. With photoevaporation times  $t_{\text{ev}} \gtrsim 100$  Myr, this process can continue down to redshifts significantly below  $z = 10$ . For stellar sources in the  $\Lambda$ CDM model, these simulations show that photoevaporation of a  $10^7 M_{\odot}$  minihalo which begins at  $z_{\text{initial}} = 9$  can take 250 Myr to finish, at  $z_{\text{final}} = 6.8$ , during which time such minihalos can survive without merging into larger halos. Observations of the absorption spectra of high redshift sources like those which reionized the universe should reveal the presence of these photoevaporative flows and provide a useful diagnostic of the reionization process.

**Dwarf Galaxy Suppression and Reionization.** As emphasized by [57], the reheating of the IGM which accompanied its reionization must have filtered the linear growth of baryonic fluctuations in the IGM, thereby reducing the baryon collapsed fraction and preventing baryons from condensing out further into the minihalos (see also [12,13,23,24,74]). A related effect, the suppression of baryon accretion onto dark matter halos, has also been studied, by 1D [33,36,37,72] and 3D simulations (e.g. [46,48,75]). The current conclusion is expressed in terms of the threshold circular velocity,  $v_c$ , below which baryonic infall and star formation were suppressed by photoionization:  $v_c \sim 30 \text{km s}^{-1}$  for complete suppression, partial suppression of infall found to extend even to  $v_c \sim 75 \text{km s}^{-1}$ . This suppression of gas accretion onto low-mass halos by the feedback effect of reionization may naturally explain why there are so many fewer dwarf galaxies observed in the Local Group than are predicted by N-body simulations of the CDM model [11].

**Acknowledgments:** I thank A. Raga, I. Iliev, and H. Martel for their collaboration on the work presented here, supported by grants NASA ATP NAG5-7363 and NAG5-7821, NSF ASC-9504046, and Texas Advanced Research Program 3658-0624-1999.

## REFERENCES

1. Abel, T., Norman, M. L., and Madau, P. *ApJ*, **523**, 66 (1999).
2. Barkana, R., and Loeb, A., *ApJ*, **523**, 54 (1999).
3. Barkana, R., and Loeb, A., preprint (2001) (astro-ph/0010468).
4. Benson, A. J., Nusser, A., Sugiyama, N., and Lacey, C. G., *MNRAS*, **320**, 153 (2001).
5. Bertoldi, F., *ApJ*, **346**, 735 (1989).

6. Bertoldi, F., and McKee, C. F., *ApJ*, **354**, 529 (1990).
7. Bertschinger, E., *ApJS*, **58**, 39 (1985).
8. Blanchard, A., Valls-Gabaud, D., and Mamon, G., *A&A*, **264**, 365 (1992).
9. Bond, J. R., Szalay, A. S., and Silk, J., *ApJ*, **324**, 627 (1988).
10. Bromm, V., Kudritzki, R. P., and Loeb, A., preprint (2000) (astro-ph/0007248).
11. Bullock, J. S., Kravtsov, A. V., and Weinberg, D. H., *ApJ*, **539**, 517 (2000).
12. Cen, R., and Ostriker, J. p., *ApJ*, **417**, 404 (1993).
13. Chiu, W. A., and Ostriker, J. P., *ApJ*, **534**, 507 (2000).
14. Ciardi, B., Ferrara, A., and Abel, T., *ApJ*, **533**, 594 (1998).
15. Ciardi, B. Ferrara, A., Governato, F. and Jenkins A., *MNRAS*, **314**, 611 (2000).
16. Ciardi, B., Ferrara, A., Marri, S., and Raimondo, G., T., *MNRAS*, submitted (2000) (astro-ph/0005181).
17. Couchman, H. M. P., and Rees, M. J., *MNRAS*, **221**, 53 (1986).
18. Dove, J. B., Shull, J. M., and Ferrara, A., *ApJ*, **531**, 846 (2000).
19. Fan, X., et al., *AJ*, **121**, 54 (2000).
20. Ferrara, A., *ApJ*, **499**, L17 (1998).
21. Giroux, M. L., and Shapiro, P. R., *ApJS*, **102**, 191 (1996).
22. Gnedin, N. Y., *ApJ*, **535**, 530 (2000).
23. Gnedin, N. Y., *ApJ*, **542**, 535 (2000).
24. Gnedin, N. Y., and Hui, L., *MNRAS*, **296**, 44 (1998).
25. Gnedin, N. Y., and Ostriker, J. P., *ApJ*, **486**, 581 (1997).
26. Griffiths, L. M., Barbosa, D., and Liddle, A. R., *MNRAS*, **308**, 854 (1999).
27. Haiman, Z., Abel, T., and Madau, P., preprint (2000) (astro-ph/0009125).
28. Haiman, Z., Abel, T., and Rees, M. J., *ApJ*, **534**, 11 (1999).
29. Haiman, Z., and Knox, L., in *Microwave Foregrounds* (ASP Conference Series) eds. A. de Oliveira-Costa and M. Tegmark, p. 227 (1999).
30. Haiman, Z., and Loeb, A., *ApJ*, **483**, 21 (1997).
31. Haiman, Z., Rees, M. J., and Loeb, A., *ApJ*, **467**, 522 (1996).
32. Haiman, Z., Rees, M. J., and Loeb, A., *ApJ*, **476**, 458 [Erratum: *ApJ*, **484**, 985] (1997).
33. Haiman, Z., Thoul, A. A., and Loeb, A., *ApJ*, **464**, 523 (1996).
34. Iliev, I. T., and Shapiro, P. R., *MNRAS*, in press (2001) (astro-ph/0101067).
35. Iliev, I. T., and Shapiro, P. R., in *20<sup>th</sup> Texas Symposium on Relativistic Astrophysics and Cosmology*, eds. J. C. Wheeler and H. Martel, in press (2001) (astro-ph/0104069).
36. Kitayama, T., and Ikeuchi S., *ApJ*, **529**, 615 (2000).
37. Kitayama, T., Tajiri, Y., Umemura, M., Susa, H., and Ikeuchi, S., *MNRAS*, **315**, 1 (2000).
38. Klein, R. I., Sandford, M. T., and Whitaker, R. W., *ApJ*, **271**, L69 (1983).
39. Lefloch, B., and Lazareff, B., *A&A*, **289**, 559 (1994).
40. Leitherer, C. et al., *ApJ*, **454**, L19 (1995).
41. Lizano, S., Cantó, J., Garay, G., and Hollenbach, D., *ApJ*, **468**, 739 (1996).
42. Madau, P., Haardt, F., and Rees, M. J., *ApJ*, **514**, 648 (1999).
43. Mellema, G., Raga, A. C., Canto, J., Lundquist, P., Balick, B., Steffen, W., and Noriega-Crespo, A., *A&A*, **331**, 335 (1997).

44. Miralda-Escudé, J., Haehnelt, M., and Rees, M. J., *ApJ*, **530**, 1 (2000).
45. Nakamoto, T., Umemura, M., and Susa, H., *MNRAS*, **321**, 593 (2001).
46. Navarro, J. F., and Steinmetz, M., *ApJ*, **478**, 13 (1997).
47. Oort, J. H., and Spitzer, L., *ApJ*, **121**, 6 (1955).
48. Quinn, T., Katz, N., and Efstathiou, G., *MNRAS*, **278**, L49 (1996)
49. Raga, A. C., Mellema, G., and Lundquist, P., *ApJS*, **109**, 517 (1997).
50. Raga, A. C., Taylor, S. D., Cabrit, S., and Biro, S., *A&A*, **296**, 833 (1995).
51. Razoumov, A., and Scott, D., *MNRAS*, **309**, 287 (1999).
52. Ricotti, M., and Shull, J. M., *ApJ*, **542**, 548 (2000).
53. Sandford, M. T., Whitaker, R. W., and Klein, R. I., *ApJ*, **260**, 183 (1982).
54. Shapiro, P. R., *PASP*, **98**, 1014 (1986).
55. Shapiro, P. R., in *The Physics of the Interstellar Medium and The Intergalactic Medium*, eds. A. Ferrara, C. F. McKee, C. Heiles, and P. R. Shapiro (ASP Conference Series, vol. 80), pp. 55–97 (1995).
56. Shapiro, P. R., and Giroux, M. L., *ApJ*, **321**, L107 (1987).
57. Shapiro, P. R., Giroux, M. L., and Babul, A., *ApJ*, **427**, 25 (1994).
58. Shapiro, P. R., Iliev, I., and Raga, A. C., *MNRAS*, **307**, 203 (1999)
59. Shapiro, P. R., and Martel, H., in *Dark Matter*, eds. S. S. Holt and C. L. Bennett (AIP Conference Proceedings 336), pp. 446–449 (1995).
60. Shapiro, P. R., Martel, H., and Iliev, I. T., to be submitted (2001).
61. Shapiro, P. R., and Raga, A. C., in *Astrophysical Plasmas: Codes, Models, and Observations*, eds. S. J. Arthur, N. Brickhouse, and J. J. Franco, *Rev.Mex.A.A. (SC)*, **9**, 292 (2000) (astro-ph/0002100)
62. Shapiro, P. R., and Raga, A. C., in *Cosmic Evolution and Galaxy Formation: Structure, Interactions, and Feedback* (ASP Conference Series, vol. 215), eds. J. Franco, E. Terlevich, O. Lopez-Cruz, and I. Aretxaga, pp. 1–6 (2000) (astro-ph/0004413).
63. Shapiro, P. R., and Raga, A. C., in *The Seventh Texas-Mexico Conference on Astrophysics: Flows, Blows, and Glows*, eds. W. Lee and S. Torres-Peimbert, *Rev.Mex.A.A. (SC)*, in press (2000) (astro-ph/0006367).
64. Shapiro, P. R., Raga, A. C., and Iliev, I. T., to be submitted (2001).
65. Shapiro, P. R., Raga, A. C., and Mellema, G., in *Structure and Evolution of the IGM from QSO Absorption Line Systems (13th IAP Colloquium)*, eds. P. Petitjean and S. Charlot (Paris: Editions Frontieres), pp. 41–46 (1997) (astro-ph/9710210)
66. Shapiro, P. R., Raga, A. C., and Mellema, G., in *Proceedings of the Workshop on H<sub>2</sub> in the Early Universe*, eds. F. Palla, E. Corbelli, and D. Galli, *Memorie Della Societa Astronomica Italiana*, **69**, pp. 463–469 (1998) (astro-ph/9804117)
67. Shapiro, P. R., Raga, A. C., and Mellema, G. 2000, *Nucl. Phys. B.*, **80**, CD-Rom 05/07 (2000)
68. Songaila, A., Hu, E. M., Cowie, L. L., and McMahon, R. G., *ApJ*, **525**, L5 (1999).
69. Spitzer, L., *Physical Processes in Interstellar Matter* (Wiley: New York) (1978).
70. Steidel, C. C., Pettini, M., and Adelberger, K. L., *ApJ*, **546**, 665 (2001).
71. Tegmark, M., Silk, J., Rees, M. J., Blanchard, A., Abel, T., and Palla, P., *ApJ*, **474**, 1 (1997).
72. Thoul, A. A., and Weinberg, D. H., *ApJ*, **465**, 608 (1996).
73. Tumlinson, J., and Shull, J. M., *ApJ*, **528**, L65 (2000).

- 74. Valageas, P., and Silk, J., *A&A*, **350**, 725 (1999).
- 75. Weinberg, D., Hernquist, L., and Katz, N. 1997, *ApJ*, **477**, 8 (1997).
- 76. Wood, K., and Loeb, A., *ApJ*, **545**, 86 (2000).